Chapter 11
Electrospun Cobalt Based Composites as Anodes for Lithium-Ion Batteries

R. Krishnapriya, Devika Laishram, Bhagirath Saini, M. J. Jabeen Fatima, and Rakesh K. Sharma

11.1 Introduction

Energy crisis and environmental pollution are the most challenging issues of this century. The growing global energy demand and the requisite of a sustainable environment triggered a renewed interest in developing very efficient methods for harvesting and storing renewable energy [1–5]. Effective implementation of these alternative renewable energy technologies (such as solar, wind, geothermal) necessitates the support of prospective energy storage systems. These include batteries, supercapacitors, and fuel cells and amongst the different possible choices, electrochemical batteries are proved to be the most accepted candidate [6]. A battery is an electrochemical device that stores electrical energy as chemical energy in its electrodes through the charging process and delivers the same as electrical energy through the discharge process when required without any gaseous emission. Among various types of batteries explored, lead-acid batteries find exceptional interest since they exhibit a relatively stable charge/discharge state. However, the large weight and volume of these batteries make them an undesirable candidate for portable, lightweight electric devices. Nickel–cadmium (Ni–Cd) or nickel–hydride (Ni–MH) based batteries, which developed later find use in mobile phones and portable electric devices, had suffered from toxicity issues and short battery life and leakage problem [7]. In this scenario, lithium-ion batteries (LIBs) benefiting from chemistry with the relatively

R. Krishnapriya (✉) · D. Laishram · B. Saini · R. K. Sharma (✉)
Sustainable Materials and Catalysis Research Laboratory (SMCRL), Department of Chemistry, Indian Institute of Technology-Jodhpur, Jodhpur, Rajasthan 342037, India
e-mail: krishnapriya@iitj.ac.in

R. K. Sharma
e-mail: rks@iitj.ac.in

M. J. Jabeen Fatima
Department of Polymer Science and Rubber Technology, Cochin University of Science and Technology, Cochin 682022, India

N. T. M. Balakrishnan and R. Prasanth (eds.), *Electrospinning for Advanced Energy Storage Applications*, Materials Horizons: From Nature to Nanomaterials,
https://doi.org/10.1007/978-981-15-8844-0_11

high energy density, power density, operating voltage, lightweight, without memory effect, outstanding rate capability, low rates of self-discharge, and low environmental pollution have accomplished remarkable developments in various advanced portable electric devices (mobile phones and laptops) as well as transportation systems like electric vehicles (EVs) and hybrid electric vehicles (HEVs) [8]. The research on LIBs began early in the 1980s and has revolutionized the portable electronics market since the first commercialization in 1990 by Sony Corp. for the Kyocera cellular phones. The key components of LIBs are anode, cathode, separators, and electrolytes. The charging and discharging of an archetypal LIB follow by a redox process in which lithium ions (Li^+-ion) shuttle among anode (negative electrode) and the cathode (positive electrode). The anode releases lithium ions into the electrolyte leading to their passage to the cathode which absorbs ions during the discharge process. The charge capacity of LIBs mainly depends on the amount of Li that can be incorporated into the electrode materials. Figure 11.1 is the schematic diagram of a rechargeable lithium-ion battery containing solid electrodes and a liquid electrolyte. In LIBs, the electrode material plays a central role in deciding battery energy/power density and cycle-life output. The most successful cathode material for LIBs is considered to be $LiCoO_2$ (LCO), which was initially reported by Prof. Goodenough et al. [9] in 1980. There are three important types of cathode materials that are widely applied in LIBs, which include olivine materials (e.g., $LiFePO_4$), spinel materials (e.g., $LiMn_2O_4$), and layered materials (e.g., $LiNi_xCo_yMn_zO_2$) [10].

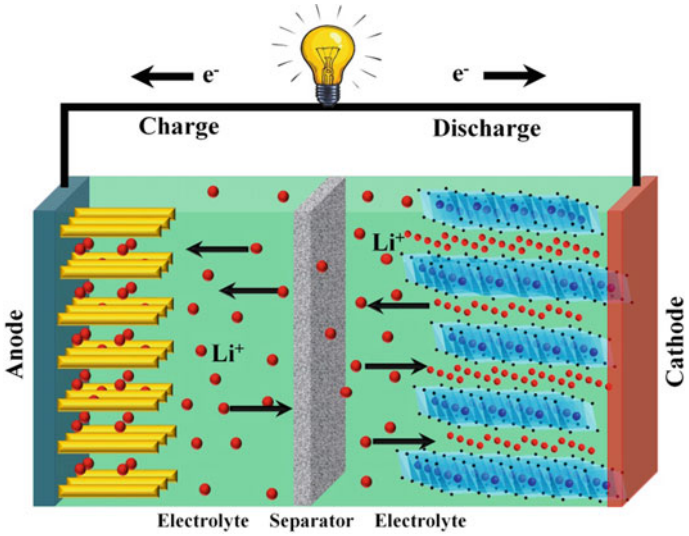

Fig. 11.1 Schematic illustration and working of lithium ion batteries

11.2 Anode Materials for Lithium-Ion Batteries

The anode plays a critical role in the entire battery performance, and it greatly relays on the physical properties (shape, size), component state, crystalline or amorphous structure, chemical properties, and energy storage capacity, etc. Owing to the low atomic weight, redox energy near to that of metallic lithium, the good theoretical capacity of 372 mAh g^{-1}, high conductivity, reversibility, and reasonably low-cost graphite has become a smart anode material in the present generation of LIBs [11]. One-dimensional (1D), two-dimensional (2D) and three-dimensional (3D) carbon-based materials, as well as porous and core-shell structures, metal alloys (Si, Sn, and Ge), Ti-based oxides ($Li_4Ti_5O_{12}$ and TiO_2) metal oxides as well as their nanocomposites, were thoroughly studied to substitute the conventional graphite which has a limited theoretical capacity of 372 mAh g^{-1} [7, 12, 13]. In order to find the wide applicability of LIBs, it is necessary to develop potential electrode materials that possess high charge/discharge rate capability and energy/power density along with reduced production/operation costs, stability, and safety [14, 15]. Such advanced functional materials fabrication requires immense scientific innovation. The development of ideal nanostructured materials undoubtedly leads to enhance capacities in terms of gravimetric or volumetric energy densities. Recently, nanotechnology is providing novel solutions and opportunities to develop many sustainable materials with predefined properties for prospective technological applications [16–18]. Nanoscale materials have absolutely substituted the traditional anode materials in most of the technological applications. Researchers found that when the size of particles inside materials reduces to match with the wavelength of electrons, phonons, and magnons, some slight size effects occur, comprising the enhancement of electrical conductivity magnetic coercivity, mechanical, optical, superparamagnetic properties owing to the large surface area. As of now, different techniques including post-templating, sol-gel, pray-drying, co-precipitation, and hydrothermal methods have been successfully demonstrated for the fabrication of functional nanomaterials for LIBs. Among the applied nano-electrode materials, 1D nanomaterials like nanowires, nanotubes, and nanofibers are getting special attention because of the considerable enhancement in charge transportation due to the quantum confinement effects [19]. The main shortcoming with the carbon anode materials is the permanent capacity loss during the first discharge-charge cycle because of irreversible side reactions with the electrolyte that leads to the formation of solid-electrolyte interfacial (SEI) layer. To avoid these issues, nanocomposites of carbon with other active materials were demonstrated, and these nano-electrode materials should be mixed with suitable binders when applied to LIBs. However, this added binder often hampers the electrical conductivity of anodes and thereby deteriorating the battery performance.

11.3 Electrospinning Process

In order to avoid severe issues of binders used for the electrode fabrication for LIBs, binder-free carbon nanofibers should be employed, and that can be fabricated via a facile electrospinning method. This technique can achieve electrode materials with solid as well as hollow interiors possessing exceptionally long length and uniform diameter with tunable composition. Such nanofiber (NF) structures are free-standing and are prepared by merely applying an electric field among the nozzle and collector while introducing the polymeric solution, as shown in Fig. 11.2 in the schematic representation [20–22]. The process of electrospinning is based on the principle of electrostatics in which the electrostatic repulsion forces in a comparatively large electrical field are used for the fabrication of nanofibers. The material to be electrospun is taken in the form of a polymeric solution and is hosted in a syringe. Later,

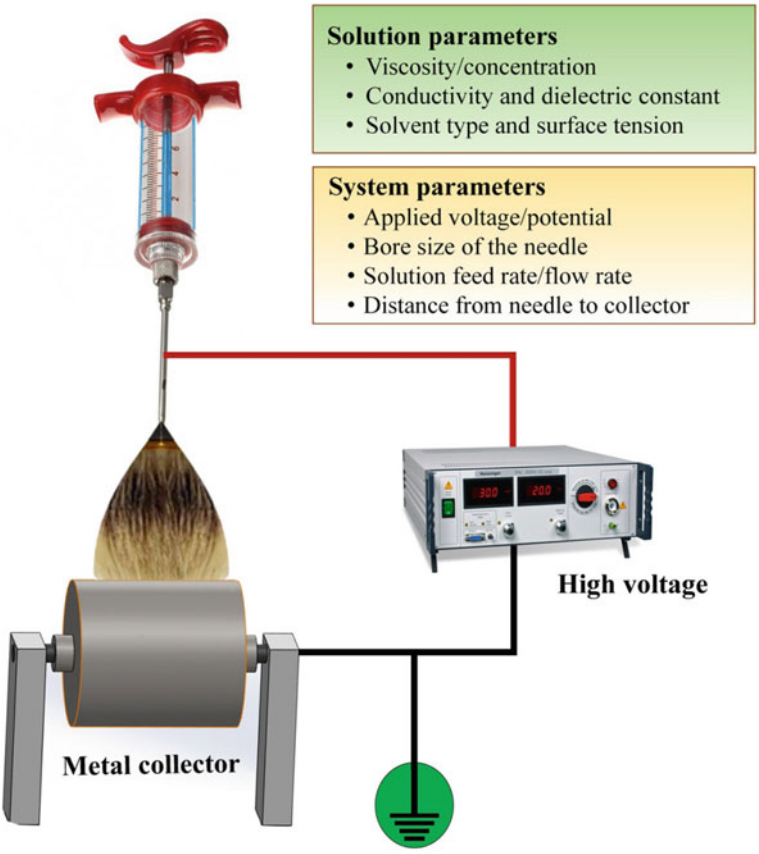

Fig. 11.2 Schematic representation of the Electrospinning process and the controllable parameters to fabricate nanofibers

a large electrical field (typically kV) is generated between the syringe nozzle and the counter electrode. When the solution is ejected through the syringe, a conical fluid-structure called the Taylor cone is created at the tip of the needle owing to the developed potential difference between the nozzle and the target [23].

At a particular voltage, the repulsive force of the charged polymer surpasses the surface tension of the solution, and a charged jet ejects from the tip of the Taylor cone. However, if the applied voltage is not large enough, the jet will break up into droplets (Rayleigh instability) [24]. Beyond the stable region, the jet erupts susceptible to bending which results in the deposition of polymer over the collector via a whipping motion. During this, the solvent evaporates which forms solid continuous nanofibers in the target [22]. As the charged solution moves towards the regions of lower potential, the evaporation of the solvent takes place that results in the high electrostatic repulsion of the charged polymer and its elongation.

The morphology and the diameter of the NFs can be tuned by careful changes of several operating parameters, including the molecular weight of the polymer used, applied voltage, solution pumping rate, spinning distance, temperature, humidity, air velocity, conductivity, viscosity, and surface tension of the solution, etc. Thus, NFs of diameters from tens to several hundred with moderately narrow size distribution can be easily fabricated. Also, this method is proved to be industry-viable, cost-effective technology, and revealed the benefits of versatility, simplicity, excellent efficiency, and yield. Moreover, the low-cost, one-step fabrication process devoid of using any hazardous chemical is found to be sustainable and can successfully be scaled up for massive production of ready to use binder-free anodes for many technological applications. The primary favorable characteristics of the electrospinning method to be used for LIBs include the tunable fiber diameter, high porosity, and specific surface area along with interconnected pore structure, which favors high electronic and ionic conductivity and is capable of enhancing the cyclability and rate capability of electrode materials [25]. By carefully choosing different polymeric blends and operational parameters, several NFs of natural polymers, polymer blends, metals, metal oxides, etc. have been spun into various NF morphologies [26–30].

11.4 Electrospun Nanofibers for Lithium-Ion Batteries

As discussed above, the electrospun NFs can apply as advanced electrode materials for LIBs with outstanding electrochemical performance, flexibility, and stretching ability. These enhanced performances are achieved through excellent conductivity due to the short ion diffusion path and a considerable length of individual NFs that can inhibit self-aggregation during the charging/discharging process. Different electrochemically active electrode materials made of carbon, metals, transition metal oxides (SnO_2, TiO_2, Fe_3O_4, MoO_2, $LiCoO_2$, CoO, $NiCo_2O_4$, and Co_3O_4), and sulphides (CuS, Cu_2S, Li_2S, MoS_2, CoS, Co_3S_4, FeS_2, Ni_3S_4) have been successfully designed and fabricated for more excellent lithium storage in LIBs [12, 31–39]. Transition metal oxides are favorable alternative anode materials owing to their high specific

capacities and lithium storage capacities in comparison to commercial graphite. When multiple components are integrated into electrospun NFs, the electrochemical performance of the nanofiber-based electrode materials can be upgraded, when compared with the single counterparts. Recently, cobalt-based nanofibers and their composite electrode materials gain special attention as anode materials. The application of cobalt-based anodes for LIBs has been significantly enhanced, and it is expected that these materials will have the capability to become commercialized shortly. Each cobalt-based compounds exhibit dissimilar electrochemical performance. The redox mechanism of the cobalt-based electrodes follows the conversion mechanism instead of the intercalation mechanism of conventional carbon materials and is generally named as conversion reaction-based anode materials for LIBs [40]. They exhibit high theoretical capacity, rich redox reaction, and favorable cyclability. So this chapter gives a brief overview of advancement in electrospun cobalt-based nanofiber composites as anode materials for LIBs application.

11.5 Structure and Properties of Cobalt Oxides

Cobalt can exhibit variable oxidation states (Co^{+2}, Co^{+3}, and Co^{+4}) as well as different coordination properties (tetrahedral, pyramidal, and octahedral) in his compounds. Subsequently, cobalt oxides offer a wide range of stoichiometric and nonstoichiometric oxides which comprising a mixed-valence state and also the oxygen vacancies. The crystal chemistry of cobalt oxides is very complex. However, these oxides are of particular interest from the other 3d metal oxides because of its ability to exist in different spin states such as low spin (LS), high spin (HS), and intermediate spin (IS), respectively.

11.5.1 Structure of Cobalt Monoxide

CoO (cobalt monoxide) generally possesses rocksalt structure at room temperature (NaCl structure), which contains Co^{2+} and O^{2-} interpenetrating fcc sublattices. It exhibits paramagnetic properties. When the temperature is below 289 K, a crystal distortion to tetragonal symmetry occurs, and it becomes antiferromagnetic. The two interpenetrating sublattices Co^{2+} and O^{2-} shifted along the body diagonal by half of its length. As a result, an individual ion is surrounded by six of the other ions. The corresponding crystal structure is given in Fig. 11.3. Each cubic unit cell consists of four Co^{2+} and four O^{2-} ions and the lattice constant of CoO is found to be 4.260 Å [41].

This material exhibits distinct electrochemical properties and has shown remarkable capacitance and excellent cyclic properties owing to the distinctive charge-discharge reactions via the formation of the Li_2O phase and consequent decomposition into Li and O species. As the charging occurs, CoO reacts with Li^+ to form

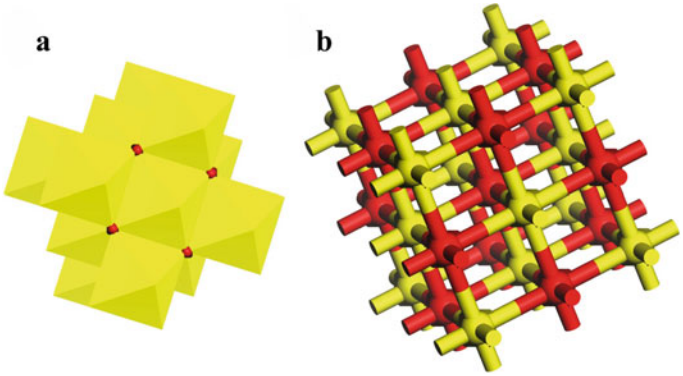

Fig. 11.3 Crystal structure of CoO consists of Co^{2+} and O^{2-} interpenetrating fcc sublattices generated using Material Studio 7.0® **a** polyhydra structure, **b** ball and stick model

metal nano-domains (M^0) dispersed in the Li_2O matrix. Whereas, during the charging steps, the M^0 and Li_2O components are transformed back to metal oxide (MO_x). This well-proved battery material is found to exhibit theoretical capacity as high as 718 mAh g^{-1} and can react reversibly with Li according to the following conversion reaction [42]:

$$CoO + 2Li^+ + 2e \rightarrow 4\,Li_2O + Co$$

Accordingly, each CoO molecule can hold two Li^+ ions per one Co ion over the reaction, which leads to greater capacity compared to the commercial graphite electrode (C_6Li) [43]. However, these anode materials often hamper the performance due to low conductivity and extreme volume change throughout the lithiation/delithiation cycles. These limitations can be overcome either by using high specific surface area nanosized electrode materials that are capable of increasing the contact area between the electrolyte and electrode materials and reducing the path length for Li-ion, which can result in a greater improvement of discharge capacities. Another approach is to fabricate the composite of CoO with highly conductive electrochemically active materials like carbon.

11.5.2 Electrospun Cobalt Monoxide for Lithium-Ion Batteries

Several composite materials of CoO with carbon, graphene, as well as NiO-CoO-carbon and CoO–graphene–carbon NFs were successfully fabricated by the electrospinning method. The electrospun composite of carbon–cobalt (C/Co) nanofibers of diameters ranging from 100 to 300 nm was studied by Wang et al. [44] when these C/Co CNFs applied as lithium storage material, a remarkable high reversible

capacity >750 mAh g^{-1}, and an excellent rate capability of 578 mAh g^{-1} at 1 C rate was obtained. The improvement in the electronic conductivity and the interfacial surface area found to have resulted from the incorporated cobalt in the fiber. The presence of cobalt in the NF increased the interfacial surface area between the carbon and liquid electrolyte, and thereby improves the electronic conductivity. The first study on highly conductive porous CoO NPs embedded in porous CNFs composite material was reported by Ryu et al. [43] The highly conductive and porous CNFs that excellently wrapped distinct CoO nanoparticles of sizes ranging from 20 to 70 nm were prepared via one-step electrospinning and successive calcination in an Ar atmosphere. The homogenous distribution of CoO all over the surface of NF can be seen in the FESEM image in Fig. 11.4.

The HRTEM images in Fig. 11.4d, f clearly exhibited CoO nanoparticles of size ranging from 20 to 70 nm and is found to be discretely embedded in the CNF. The CoO embedded CNFs exhibited a high capacity of 853.5 mAh g^{-1}, stable cycling during 100 cycles with a high coulombic efficiency of over 99%, and high rate capability even at a rate of 20 C by a reversible conversion reaction of CoO nanoparticles and facile electron transport through highly conductive CNFs. It is found that the greater LIB performance is due to the combined effect of nanosize CoO particles, which is responsible for providing reversible and facile Li insertion and extraction along with conductive CNF backbones, capable of providing 1-D electron transport path and further available capacity. Zhang et al. [45] fabricated CoO–C nanofibers with the homogeneous distribution of CoO NPs with network structure by electrospinning of cobalt(II) acetate and polyacrylonitrile. The morphology of the NFs was networks structured, and after these electrode heat-treated at 650 °C, it showed a remarkable discharge capacity as high as 633 mAh g^{-1} even after 52 cycles at a current density of 0.1 A g^{-1}. The propitious properties are found to be owing to the superior structural stability of CoO nanoparticles in CNF and by the better conductance arising from the CNF and the resultant network-based structure. The flexible mats like CoO–graphene–carbon NFs were also synthesized via electrospinning followed by careful heat treatment [46]. The graphene precursor was carefully treated to get good dispersion in the N, N-dimethylformamide (DMF) solvent. The resulted amount of graphene and CoO in the fabricated nanofibers was comparatively less. Still, the material exhibited a reversible capacity of 690 mAh g^{-1} after 352 cycles at a current density of 500 mAg^{-1} (Fig. 11.5). The resultant improvement was found to be attributed to many factors such as the microstructure with large pores that provided the effective diffusion of Li^+ ion, high conductivity of mats which allows easy transfer of electrons as well as decrease the polarization. Remarkably, the graphene in the composite is found to control the particle size of CoO NPs and thereby provided excellent structural stability against fracture. The binder-free anodes reduced the internal resistance and are capable to provide a high output voltage. Moreover, the CoO and graphene introduced active defect sites into the CNF mats that improved the capacity of Li^+ storage. Another significant work that explains the direct growth of NiO–CoO nanoneedles on carbon fibers by a simple solvothermal strategy to fabricate nanobrushes [47].

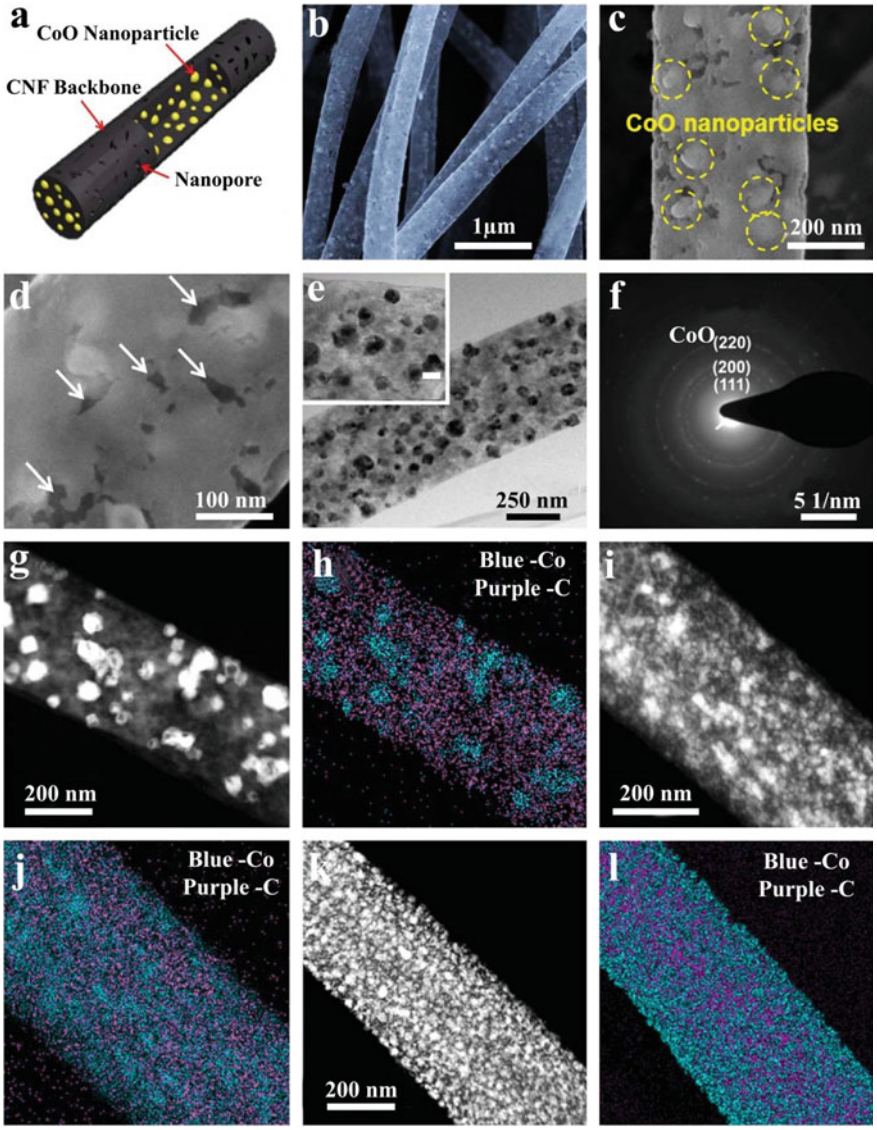

Fig. 11.4 **a** Schematic illustration of a CoO embedded CNF; **b**–**d** (SEM) images of CoO embedded CNFs calcined with a Co precursor/PAN ratio of 0.4 (Co precursor: 0.2 g); **e** HRTEM images and **f** SAED pattern of the CoO embedded CNF; **g** STEM image of the CoO embedded CNF; and **h** atomic distribution of cobalt and carbon analyzed from the STEM image in (**g**). STEM images of Co/CoO nanoparticles embedded in CNFs calcined with different ratios of Co precursor/PAN: **i** 1 (Co precursor: 0.5 g) and **k** 2 (Co precursor: 1 g); **j**, **l** atomic distribution of Co (blue color) and C (purple color) analyzed from the STEM images in (**i**) and (**k**), respectively; Co precursor/PAN ratios of (**j**) 1 and (**l**) 2. Reproduced from Ref. [43] with the permission from Royal Society of Chemistry

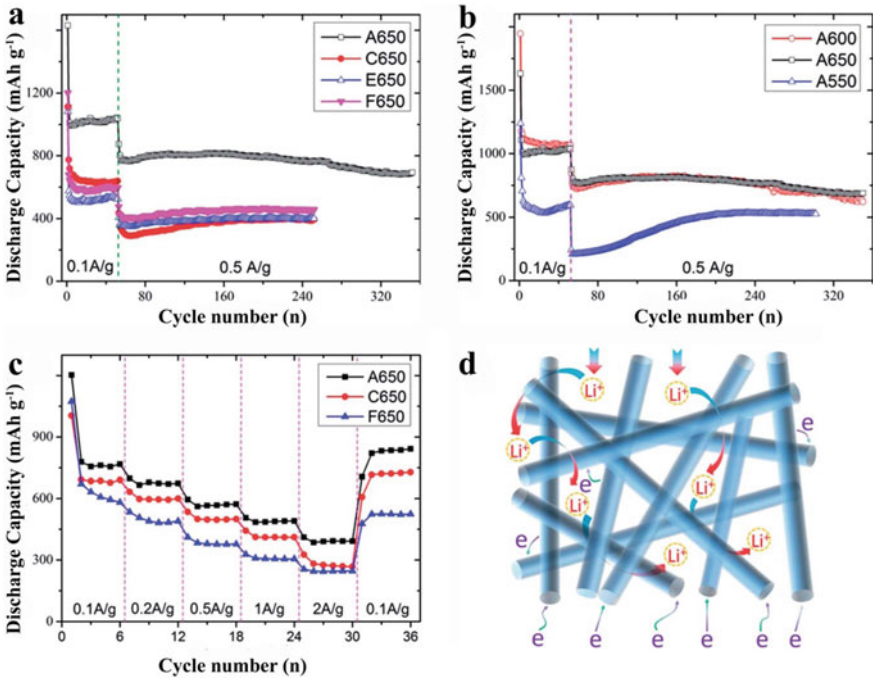

Fig. 11.5 **a** The cyclic properties of samples A650 (CoO-G-C), C650 (CoO-C), E650 (pure carbon), and F650 (graphene-carbon). **b** The discharge capacity vs. cyclic number curves of the samples A650, A600, and A550. **c** The rate capacity of the samples A650, C650, and F650. **d** A schematic diagram to show that the A650 nanofiber flexible mats are of benefit for the storage of Li^+. Reproduced from Ref. [46] with the permission from Royal Society of Chemistry

By changing the solvents from water to absolute ethanol, and finally to isopropanol, the density of nanobrushes was found to change drastically. This can be clearly observed in the SEM images of fabricated fibers in Fig. 11.6. The elctrospinned carbon fibers (Fig. 11.6a) show an interconnected continuous framework with 300–400 nm diameters. After the fibers were allowed to undergo the hydrothermal process, the surface of the fibers was effectively covered with disordered NiO–CoO nanoneedles by utilizing water as a solvent, as revealed in Fig. 11.6b. Particularly, the mixed water and absolute ethanol solvent resulted in the formation of brush-like NiO–CoO/carbon fiber composites with strong adherence to the carbon fiber substrates, as evident in Fig. 11.6c. In this study, the solvent ethanol and isopropanol were responsible for altering the morphology of NFs by reducing the surface tension and to modify the polarity and coordination potentiality of the solvent used. Thus, the nucleation and growth of nanoneedles were effected resulted in distinct morphology, as shown in the SEM image.

The particular study also reported detailed time-dependent electrospinning experiments to illustrate the mechanism of NiO–CoO/carbon fiber nanobrushes formation. The NiO–CoO/carbon fiber nanobrushes synthesized using ethanol as a solvent

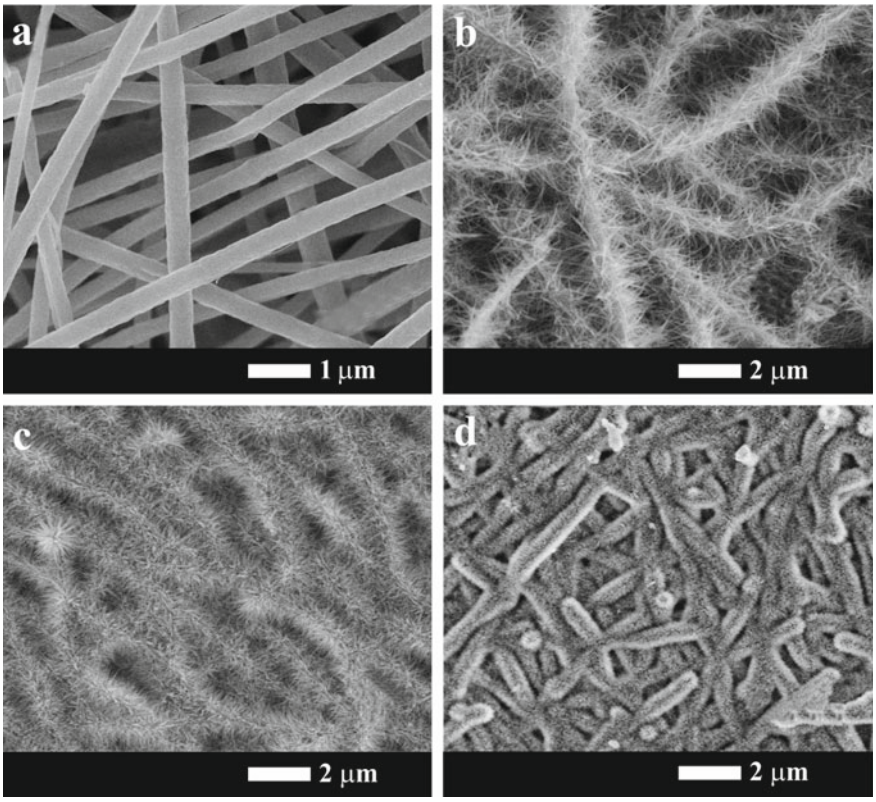

Fig. 11.6 SEM images of **a** pure carbon fibers, **b** sample synthesized water, **c** sample synthesized absolute ethanol, **d** sample synthesized isopropanol. Reproduced from Ref. [47] with permission from American Chemical Society

showed the discharge capacity as large as 801 mAh g^{-1} after 200 cycles at a current density of 200 mAg^{-1}. The electrode showed an initial discharge capacity of 961.53 mAh g^{-1} with a charge capacity of 692 mAh g^{-1}, demonstrating an irreversible capacity loss of about 38% which can be understood from Fig. 11.7. A long stable voltage stage at 1.0 V in the first discharge is exhibited by the electrode, which is found to be due to the complex phase alteration of CoO–NiO to Co–Ni and also due to the solid–electrolyte layer (SEI) formation. The obtained enhanced Li^+ storage ability and high cyclic performance for the NiO–CoO/carbon fiber is due to the high surface area, large porosity, and excellent electric conductivity of carbon fibers as well as the superior properties of NiO–CoO nanoneedles. Particularly in the presence of NiO along with unique electroactive material CoO, the better electrochemical performance was exhibited for LIBs than the single metal oxide. The interconnected NiO–CoO structures that could act as the highway for electrons and the interfacial space formed between NiO and CoO nanoneedles that is capable of accommodating

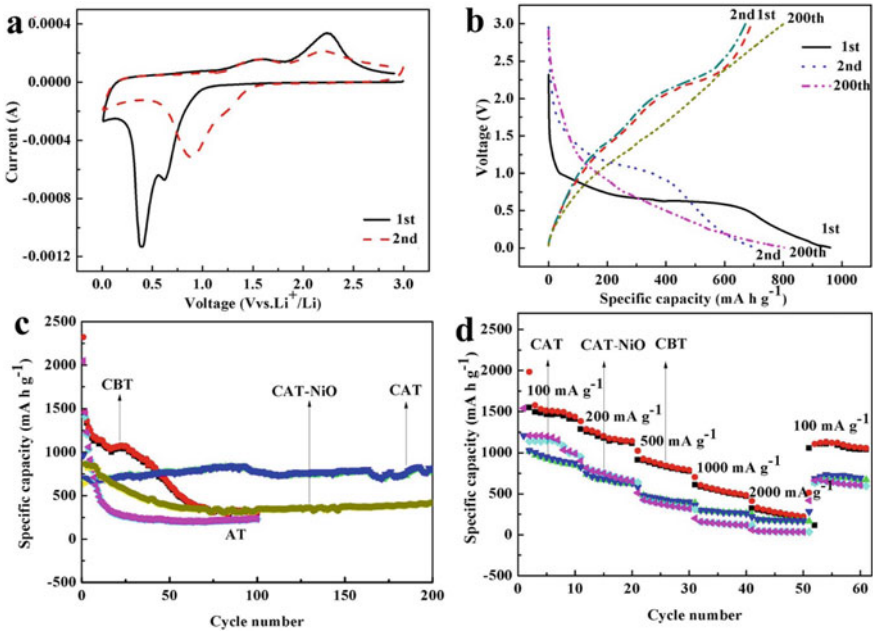

Fig. 11.7 **a** CV curves of NiO–CoO/carbon fiber nanobrushes between 0.01 and 3.0 V at the sweep speed of 0.1 mv/s, **b** Charge–discharge curves of NiO–CoO/carbon fiber nanobrushes at a current density of 200 mAg^{-1}, **c** Cycling performances of NiO–CoO/carbon fiber nanobrushes before and after heat treatment (CBT and CAT), NiO–CoO nanosphere electrode (AT), and NiO/carbon fiber nanobrushes (CAT-NiO) at 200 mAg^{-1}, respectively. **d** Rate-capability properties of NiO–CoO/carbon fiber nanobrushes before and after heat treatment (CBT and CAT) and NiO/carbon fiber nanobrushes (CAT-NiO at different current densities). Reproduced from Ref. [47] with permission from the American Chemical Society

the substantial volume change and also provided high structural stability towards the fracture.

Thus, CoO NFs has proved to be a prospective candidate for binder-free, self-standing NFs for LIBs applications, and Table 11.1 provides comprehensive electrochemical progress of CoO NF anodes for LIBs.

Table 11.1 Performance of electrospun CoO NFs for LIBs

Material	Capacity ($mAh\ g^{-1}$)	Cycles	Current density (mAg^{-1})	References
CoO–CNF	853.5	100	140	[43]
C/Co–CNF	800	50	100	[44]
CoO–C–NF	633	52	100	[45]
CoO–graphene	800	100	500	[46]
NiO–CoO–C	801	200	200	[47]

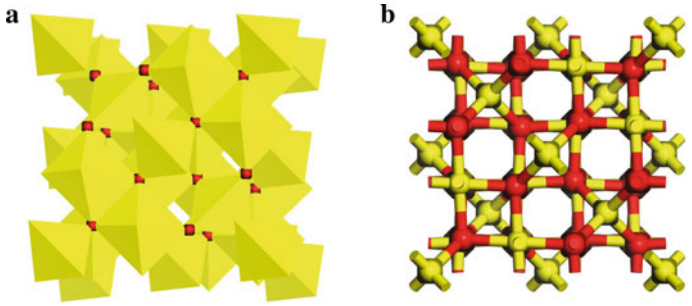

Fig. 11.8 Crystal structure of Co_3O_4 generated using Material Studio 7.0® **a** polyhydra structure, **b** ball and stick model

11.5.3 Structure of Cobalt (II, III) Oxide

Co_3O_4 is the thermodynamically favored form of cobalt oxide, which belongs to a normal cubic spinel with the Fd3m space group. Compared to CoO, the structure of Co_3O_4 is complicated with two types of Co ions tetrahedrally coordinated Co^{2+}(II) and octahedrally coordinated Co^{3+}(III), which is represented in Fig. 11.8. The distance of Co-O is 1.929 Å for the tetrahedrally coordinated species and 1.916 Å for the octahedrally coordinated species. The unit cell of Co_3O_4 consists of 8 Co^{2+}, 16 $Co^{3+,}$ and 32 O^{2-} ions, respectively which provides a very large unit cell with 56 atoms. [40] The structure can also be defined as the stacking of two kinds of polyhedral layers along the $< 111 >_c$ direction of the cubic cell. Furthermore, when Li^+ ions are inserted into $Co_3O_{4,}$ the natural black color of this material is changes to light yellow. Hence this material is applied as the most active material of cobalt.

11.5.4 Electrospun Cobalt (II, III) Oxide as Anodes for Lithium-Ion Batteries

Co_3O_4 is regarded as a competent anode material for LIBs owing to its high theoretical specific capacity of 890 mAh g^{-1} compared to commercial graphite (372 mAh g^{-1}) [48]. The material possesses a spinel structure with a Co^{2+} located in a tetrahedral coordination site and Co^{3+} located in an octahedral site. From the DFT calculations, the calculated bandgap is 1.96 eV. Owing to its wide bandgap, the electrical conductivity of this material is found to be very low, and thus material suffers from large volume change upon cycling resulting in low coulombic efficiency, low rate capability, and finally poor cycling stability. These material demerits are mainly due to the pulverization and deterioration of the electrode materials while lithiation and delithiation steps. The mechanism of operation follows the reversible conversion reaction lead to the storage of 8 mol of Li per mole of Co_3O_4 according to the following reaction:

$$Co_3O_4 + 8Li^+ + 8e \rightarrow 4Li_2O + 3CoCo_3O_4 + 8Li^+ + 8e \rightarrow 4Li_2O + 3Co$$

The effective way to overcome the material inefficiency is to prepare nanometer-sized materials with designed structures or to disperse the Co_3O_4 uniformly into carbon matrix such as activated carbon, active carbon coatings, carbon nanotubes (CNTs), and also graphene. Since the homogenous dispersion of Co_3O_4 in the carbon matrix can deliver high electrical conductivity and high cyclic stability benefited from carbon. Such composites are effectively synthesized by a one-step electrospinning technique and delivered a significant high capacity in the range of 800-952 mAh g^{-1} after 100 cycles with provided current density of 100 mAg^{-1}. An et al. [48] successfully synthesized CNF/Co_3O_4 nanopyramid core-shell nanowires (NWs) by following electrospinning, reduction, and hydrothermal methods. The FESEM images confirmed the uniform formation of the Co_3O_4 composites with CNF and CNF/Co_3O_4 nanopyramid core-shell NWs as shown in Fig. 11.9.

The FESEM image of the material exhibited smooth surfaces of CNFs with diameters in the range of 208–224 nm and revealed a uniform morphology. Figure 11.9d clearly shows the electrode material is composed of octahedral Co_3O_4 and CNFs in which the CNFs penetrated the octahedral Co_3O_4. The resultant interface formed

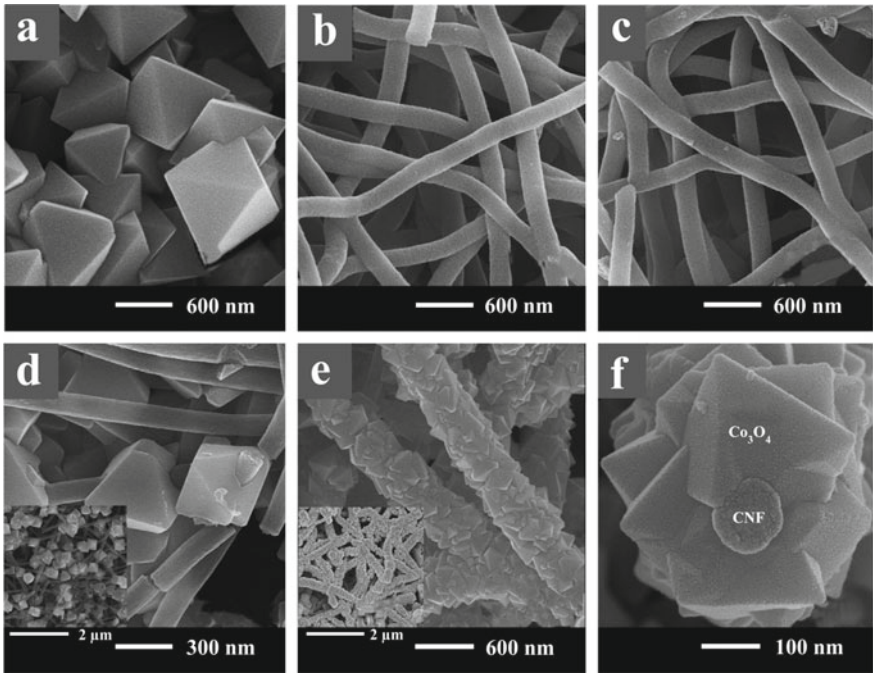

Fig. 11.9 SEM images of **a** octahedral Co_3O_4, **b** conventional CNFs, **c** CoO seeds/CNFs, **d** Co_3O_4/CNF composites, and **e** CNF/Co_3O_4 nanopyramid core shell NWs. **f** A cross sectional SEM image obtained from CNF/Co_3O_4 nanopyramid core shell NWs. Reproduced from Ref. [48] with permission from the Elsevier

between the CNFs and Co_3O_4 nanopyramids is well connected, and that is capable enough to contribute the enhanced electron transfer. The LIBs fabricated using CNF/Co_3O_4 nanopyramid core-shell NWs showed an exceptional discharge capacity of 1173 mAh g^{-1} after the first cycle and 795 mAh g^{-1} after 50 cycles. The obtained initial coulombic efficiency of 84.8% and rate capability of 570 mAh g^{-1} at 700 mAg^{-1} made this composite much suitable for LIB application. The excellent electrochemical performance exhibited by this material is due to the synergistic effect of 1-D CNFs that offer effectual electron transport and the geometric network structures which facilitate easy diffusion of Li-ion. Abouali et al. did another significant work. [49], reported a facile one-pot synthesis approach to fabricate porous carbon nanofibers (PCNF) integrated with Co and Co_3O_4 NPs embedded CoO_x/PCNF. The adopted synthesis method favored the bounding of spherical Co_3O_4 NPs with graphitic carbon shells in the CNF matrix by careful control of reaction parameters. The composite electrodes exhibited a remarkable capacity of 952 mAh g^{-1} after 100 cycles at a current density of 100 mAg^{-1}. The layers of graphene around each Co_3O_4 NPs provided an uninterrupted conductive network inside the conductive CNFs, resulted in an effective decrease of the ion/electron inter transfer resistance. Such a structure also helped to reduce the detachment of NPs from the CNF during the charge-discharge process and facilitated to retain the stable structure features. Another remarkable work was the fabrication of the hierarchically mesoporous flower-like Co_3O_4/carbon nanofiber (Co_3O_4/CNF) composites with a shell–core structure and its application as the anode material for LIBs [50]. The synthesis method involved the preparation of CNF by electrospinning followed by the electrophoretic deposition of Co_3O_4 and finally annealing in air. The morphological analysis revealed the formation of flower-like Co_3O_4 shell around the CNF core that delivers a porous, high surface area with copious inner spaces through the mesopores that enabled the easy diffusion of Li^+ and avoided the volume expansion to result in high specific capacities. The particular 1D pathway increased the rate capability and also offered good electrical conductivity as well as structural stability. The fabricated LIBs provided initial capacity as high as 1446 mAh g^{-1} and the specific capacity 911 mAh g^{-1} without capacity fading after many cycles. Later, Hu et al. [51] fabricated composite of porous Co_3O_4 NF coated with reduced graphene oxide (GNS) as a surface-modification layer to facilitate better interconnection, ability to sustain volume change, to avoid the aggregation of metal NPs and to facilitate rapid transport of Li^+ ion during charge/discharge cycling. The fibers with pore structure-function as the paths for fast electrolyte transport to the electrode. The ultrafine Co_3O_4 NCs in the fibers with grain boundaries/interfaces offered a large material/electrolyte contact area, short diffusion distance for Li^+ ions, and enabled the rapid lithiation/delithiation. Moreover, the unique porous architecture was interconnected by Co_3O_4 NCs and the rGO sheets deliver the volume changes and avoiding the agglomeration of fibers during the electrochemical reactions. Thus, the fabricated electrodes of Co_3O_4@rGO material displayed high Coulombic efficiency, high cyclic stability, and high rate capability of 900 mAh g^{-1} at 1 A g^{-1}, and 600 mAh g^{-1} at 5 A g^{-1}. Recent modification on anode material is the use of a highly porous zeolite type metal-organic framework (MOF) named as ZIF-67 to synthesize cobalt-based composites through

electrospinning. Zhang et al. [52] fabricated carbon-based hierarchical porous fiber composite with uniformly distributed hollow Co_3O_4 NPs via electrospinning of ZIF-67 NPs. When the fabricated electrodes were applied for LIBs, it is found that the micropores and Co_3O_4 yielded high-density active sites. Simultaneously, the macropores in the electrode surface offered a superior mass/charge transports through the electrodes, as shown in Fig. 11.10.

Another work explored a controllable electrostatic spinning to synthesize1D Co_3O_4 nanotubes at large-scale that yielded Co_3O_4 nanotubes with tightly packed NPs as primary building blocks. The fabricated LIBs showed a high specific capacity and cycle stability of 856.4 mAh g^{-1} at 0.25 C and 677.2 mAh g^{-1} at 1 C for up to 60 cycles [53]. The Co, N-doped carbon materials can be formed by thermal treatment and the CNFs derived by this approach that exhibited high surface area, hierarchical pores, and high nitrogen content. Moreover, the presence of Co and N can catalyze the graphitization of carbon, which is highly desirable for enhancement in conductivity. The more defects created around the pores during the heat treatment process can effectively increase the layer space by the presence of cobalt. In a recent study, Liu et al. [54] modified the electrospinning method with sol-gel synthesis to prepare

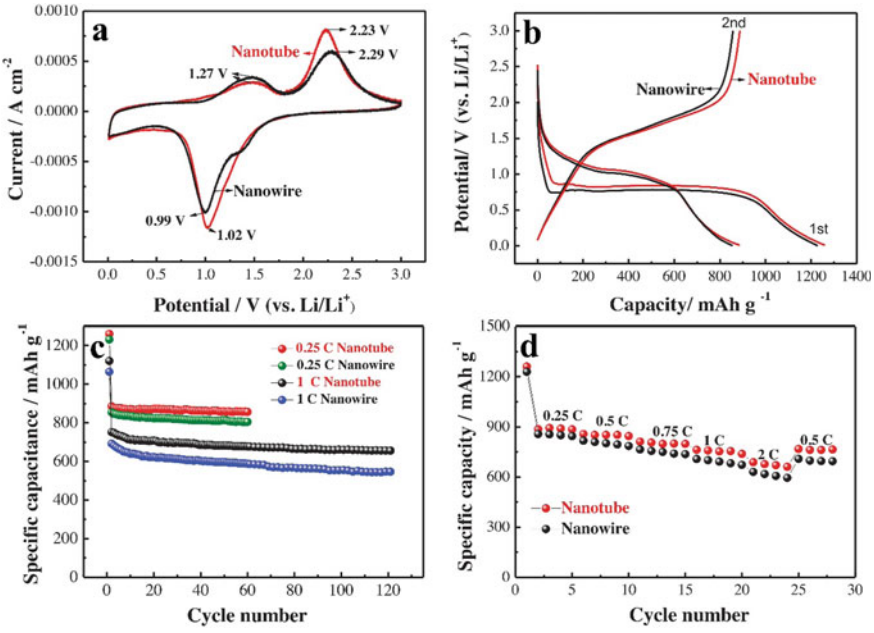

Fig. 11.10 **a** CV curves of Co_3O_4 NTs and NWs at the second cycle at a scan rate of 0.1 mV s^{-1} in the potential range 0–3.0 V (vs. Li/Li^+); **b** Charge/discharge profiles of Co_3O_4 NTs and NWs electrodes between 0.01 and 3.0 V at 0.25 C; **c** Nyquist plots of the Co_3O_4 NTs and NWs electrodes after 10 cycles in the frequency range from 100 kHz to 10 MHz; **d** Cycling performance of Co_3O_4 NTs and NWs at 0.25 C and 1 C; **e** Rate performance of Co_3O_4 NTs and NWs. Reproduced from Ref. [53]. with permission from the Elsevier

Table 11.2 Performance of electrospun Co_3O_4 NFs for LIBs

Material	Capacity (mAh g^{-1})	Cycles	Current density (mAh g^{-1})	References
CNF/Co_3O_4 nanopyramid core-shell NWs	795	50	100	[48]
Co_3O_4–PCNF	952	100	100	[49]
Co_3O_4/CNF	911	50	200	[50]
Co_3O_4@rGO	967	100	100	[51]
Co_3O_4@CPNF	1100	200	100	[52]
Co_3O_4 NT-NP	856.4	60	0.25C	[53]
Co_3O_4@NFs	330	170	0.5C	[54]
Co_3O_4@CNFs	400	200	0.5C	[54]

Co_3O_4@nanofibers (NFs) and Co_3O_4@carbon NFs (CNFs). The hollow 3D network nanostructure obtained with tiny well-dispersed Co_3O_4 NCs on the surface that could effectively avoid the aggregation. Stable cyclic performance with Li storage capacity of 330 and 400 mAh g^{-1} after 170 and 200 cycles obtained for Co_3O_4@NFs and Co_3O_4@CNFs, respectively. The study revealed that through electrospun carbon coating layer, the internal resistance was decreased by increasing electrical conductivity which resulted in an enhanced energy storage performance of LIBs. Table 11.2 summarize the progress of Co_3O_4 NF anodes for LIBs.

11.5.5 Ternary Oxides of Cobalt as Anodes for Lithium-Ion Batteries

Owing to the high lithium redox potential while using Co_3O_4, many efforts have been made by scientists to substitute the Co ion in Co_3O_4 with low-cost and eco-friendlier metal ions such as Zn, Cu, Ni, Mn, and Fe to form potential anode materials for LIBs which include $ZnCo_2O_4$, $CuCo_2O_4$, $NiCo_2O_4$, and $MnCo_2O_4$. These mixed transition metals with stoichiometric or non-stoichiometric compositions have gained copious consideration due to their fascinating electrochemical properties such as high theoretical specific capacitance, and variable oxidation states. These are generally denoted by $A_xB_yO_z$ with two metal elements of A, B = Co, Ni, Zn, Mn, Cu, Fe, Mo, etc. and both A and B play substantial roles in electrochemical energy storage devices. Depending on the ratio of A/B/O, transition metal oxides (TMOs) can be mainly classified into three groups: AB_2O_4, $ABO_{2/3/4}$, and $A_3B_2O_8$. [55] Therefore, the crystal structures of each type of TMOs are found to vary which results in different physical and chemical properties, and accordingly, their battery performances. Generally, the single-phase ternary metal oxides possessing a spinel structure consist of two different cations with variable oxidation states within their octahedral and tetrahedral sites. This specific structure facilitates the perfect tuning of its physical and

chemical features. Consequently, the material shows higher electrical conductivity than simple transition metal oxides due to comparatively low activation energy for charge transfer among the two different cations [56]. Furthermore, such chemical compositions result in high electrochemical activities thereby could contribute to a great specific capacity.

Spinel AB_2O_4 electrode materials for LIBs can be again classified as spinel metal-cobalt oxides (ACo_2O_4, A = Ni, Zn, Cu, etc.), spinel metal-ferrum oxides (AFe_2O_4, A = Ni, Co, Mn, etc.), and spinel metal-manganese oxides (AMn_2O_4, A = Ni, Co, Zn, etc.) Amongst these spinel metal-cobalt oxides have been studied extensively in which specifically $NiCo_2O_4$ gains particular attention for its high theoretical capacity, benign environmental nature, cost-effectiveness, and also the earth-abundance. $NiCo_2O_4$ is an inverse spinel oxide with the nickel ions occupying the octahedral sites, and half of the cobalt ions occupying the tetrahedral sites and the other half ions hold the remaining octahedral sites [57]. When applied to LIBs, $NiCo_2O_4$ material has shown high specific capacity as high as 891 mAh g^{-1}, good conductivity, and low diffusion resistance between Li^+ ions and the electrolyte. Zhou et al. [58] reported the tufted $NiCo_2O_4$ nanoneedles hydrothermally grown on electrospun carbon nanofibers as anode material for LIBs. The unique three dimensional (3D) hybrid morphology of synthesized composite looks as if clustered acicular leaves on branches. A reversible discharge specific capacity of 1033.6 mAh g^{-1} at a current density of 200 mAg^{-1} was achieved even after 250 cycles with the coulombic efficiency >98%. The obtained high specific capacity is mainly attributed to the unique 3D morphology and the synergetic effects of hybrid CNFs. Zhu et al. [59] modified the $NiCo_2O_4$ electrode material with Au NPs. The $NiCo_2O_4$@Au nanotubes (NTs) having a mesoporous structure with hollow interiors, and these nanotubes were synthesized by the electrospinning followed by calcination in air. The composite electrode showed high reversible capacity of 732.5 mAh g^{-1} even after 200th cycles at a current density of 100 mAg^{-1} with excellent cycling stability. The embedded Au NPs penetrated the whole electrode to form 3D percolation networks and also acts as adhesion centers/mechanic anchoring points to firmly hold $NiCo_2O_4$ particles, which is capable of giving the required tolerance ability against electrode to volume expansion as shown in Fig. 11.11. An electrospun binder-free carbon fiber hybrid with Ni–Co also synthesized and applied to LIBs that have demonstrated the highest capacity of 734 mAh g^{-1} at a current density of 150 mAg^{-1} [60]. This binder-free electrode provided better interconnection by carbon fibers, which also gave a highly conductive path for effective charge transfer. Furthermore, the highly dispersed Ni–Co compounds are proved to be capable of resisting the volume change during charging and discharging and successfully maintained the electrode reliability.

Other notable work reported was the preparation of uniform $NiCo_2O_4$ nanotubes (NCO-NTs) through electrospinning followed by calcination in the air by Li et al. [35], and these NTs were successfully used as anode materials for LIBs as well as Sulphur ion batteries (SIBs). The exceptional long-term electrochemical stability and reversibility obtained with retention of 93.6 % of specific capacitance even after 3000 cycles with the advantage of the distinct porous structure with hollow 1D morphology of NCO-NTs. The unique morphology of NCO-NTs provided high surface area as

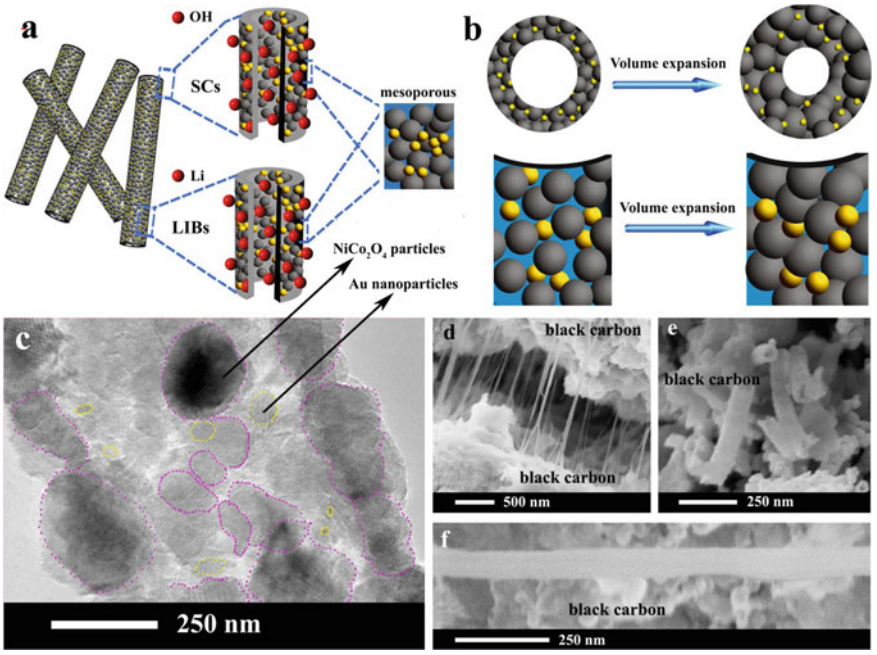

Fig. 11.11 **a** Schematic representation of the electrolyte/electrode interface for LIBs and SCs; **b** illustration of volume change of $NiCo_2O_4$@Au NTs before and after cycle; **c** TEM images of a single $NiCo_2O_4$@Au NT; **d**, **e** SEM image for the SCs of the $NiCo_2O_4$@Au NT electrodes after 10,000 cycles; and **f** SEM image for the lithium ion batteries of the $NiCo_2O_4$@Au NT electrodes after 200 cycles. Reproduced from Ref. [59] with the permission from Elsevier

well as efficient transport pathways for rapid electron transport thereby capable of enhancing the electrochemical kinetics. Mainly, the hollow structures ascertained to serve as ion-buffering reservoirs for OH^- ions and also capable of adjusting the volume change occurs by insertion and extraction of the OH^- ions. Thus, offer minimum diffusion distance to the interior surfaces, increased contact area between electrolyte to the electrode, more active sites for rapid faradaic redox reactions. A porous $ZnCo_2O_4$ NTs as anode materials for LIBs are reported for the first time by Luo et al. [61] by the electrospinning method followed by thermal annealing in air. The fabricated NTs were polycrystalline and consisted of both interconnected NCs and many nanopores in the tube walls. Such NTs when applied as anode materials for LIBs, offered a high reversible capacity of 1454 mAh g^{-1} at a current density of 100 mAg^{-1}, and even keeps 794 mAh g^{-1} at 2000 mAg^{-1} after 30 cycles. Such a unique structure facilitated fast Li-ion transport with the volume expansion/contraction during Li insertion/extraction processes. Chen et al. [62] described a simple, cost-effective, and scalable approach for the fabrication of CNFs by electrospinning and thereby anchoring these NFs with $Zn_xCo_{3-x}O_4$ (ZCO) nanocubes, which involved a hydrothermal process followed by thermal treatment. Fabricated anodes delivered high reversible capacity around 600 mAh g^{-1} at a current density

of 0.5 C following 300 charge-discharge cycles. The authors found that the obtained superior electrochemical performance was accredited to the controllable size of the ZCO nanocubes and synergistic effects between ZCO and the CNFs. It is found that even after the 150 cycles, discharge capacities as high as 656 and 390 mAh g^{-1} were obtained which was much higher than the reported value of 372 mAh g^{-1} for graphite electrode. Another significant ternary cobalt-based metal oxide applied to LIBs is $CoMn_2O_4$. Yang et al. [63] fabricated hollow nanofibers of $CoMn_2O_4$ by electrospinning method. These materials also exhibited good lithium storage performances with high specific capacity and excellent reversible capacity of 526 mAh g^{-1} at a current density of 400 mAg^{-1} after 50 cycles. The unique 1D shape with the porous structure not only offered smooth electron transport pathways but also could provide enough void spaces to endure the volume change during the charge-discharge process. Hwang et al. [64] reported the synthesis of both $MnCo_2O_4$ (MCO) and $CoMn_2O_4$ (CMO) mesoporous hollow nanofibres by electrospinning and highly exothermic combustion reactions in the air. They have found the mechanism of formation of such fiber differs from the earlier reported heterogeneous contraction mechanism [65]. From the thermal analyses and structural investigation, the authors found the formation pathways of single- and double-walled hollow fibers via combustion reactions, which principally depends on the ramping rate during heat-treatment. The SEM and TEM images of Fig. 11.12 clearly shows the formation of single and double walled fibers with hollow interiors.

The high discharge capacity of 997 and 798 mAh g^{-1} were obtained for the electrodes even after the 50th cycle with a coloumbic efficiency as high as 98 and 99%. Moreover, superior charge capacity retention at various current densities and the highest current density of 5 C, the charge capacity of 696 and 575 mAh g^{-1} were achieved. The excellent lithium storage capacity and good cycling performance and rate capability for LIBs were ascribed to the large surface area, the void space that is originating from the hollow morphology which enabled to provide more active sites for Li^+ storage and easy Li^+ transportation during charge-discharge cycles. Table 11.3 summarize the electrode performance of ternary oxide NFs used for LIBs application.

11.6 Conclusion

The electrospinning approach is recognized as a very versatile methodology to fabricate various composite anode materials with tuneable morphologies, hybrid, and interconnected 3D network structures that are capable of enhancing the electrochemical performance through facile electron transfer. The achieved remarkable advancement of LIB technology would not have been conceivably deprived of the progress of many nanocomposites and nanometer-thick coatings, which is accountable to optimize the ionic and electronic conduction pathways and even to obstruct unsought and irreversible side reactions. Advances in electrospinning of cobalt-based composites

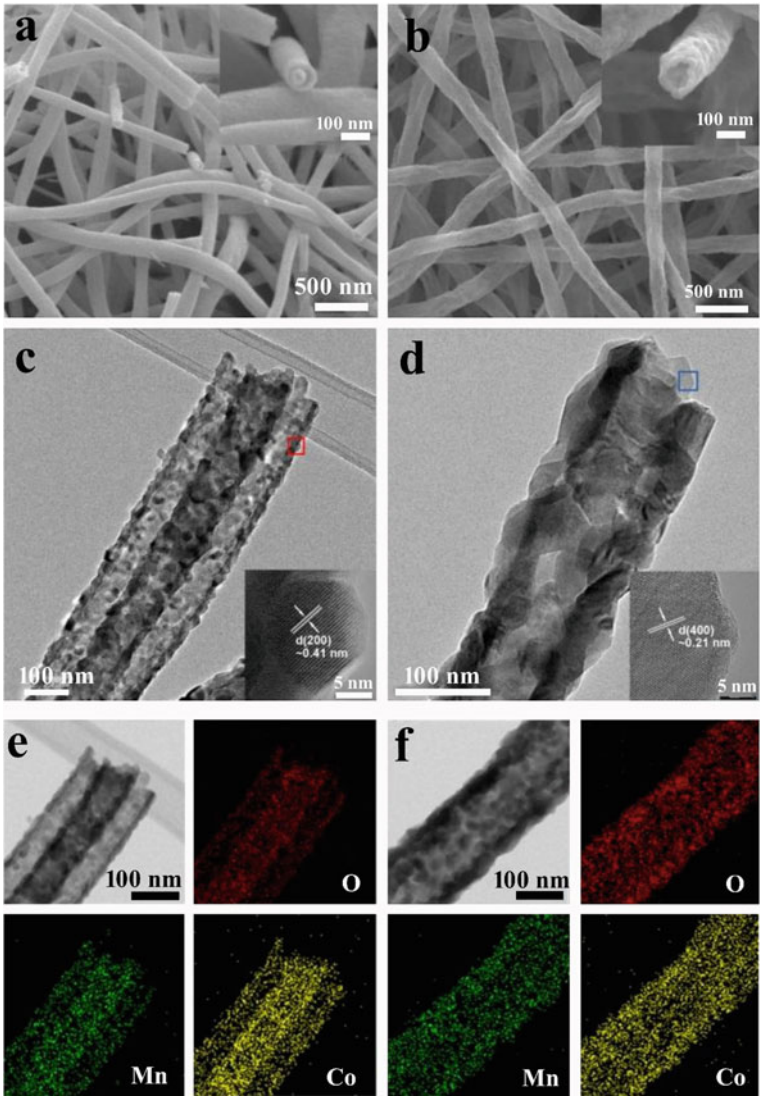

Fig. 11.12 **a**, **b** SEM, **c**, **d** TEM, and **e**, **f** EDS mapping images of MCO fibres annealed at different heating rates of 0.5 °C min^{-1} (**a**, **c**, **e**) and 5 °C min^{-1} (**b**, **d**, **f**). The insets in **a**, **b** show cross-sectional images of representative hollow fibres, and those in **c**, **d** are HRTEM images of the regions marked by squares; **e**, **f** present the elemental distributions of O, Mn, and Co. Reproduced from Ref. [64] with permission from the Royal Society of Chemistry

Table 11.3 Performance of electrospun ternary oxide NFs for LIBs

Material	Capacity (mAh g^{-1})	Cycles	Current density (mAg^{-1}) or C	References
Tufted $NiCo_2O_4$ on CNF	1033.6	250	200	[58]
$NiCo_2O_4$@Au–CNF	732.5	200	100	[59]
$NiCo_2O_4$	595	100	100	[60]
$NiCo_2O_4$ NTs	1454	30	100	[61]
$Zn_xCo_{3-x}O_4$	600	300	0.5C	[62]
$CoMn_2O_4$ hollow nanofibers	526	50	400	[63]
$MnCo_2O_4$	696	50	5C	[64]

have demonstrated that the technique affords us a remarkably simple and versatile approach for the preparation of composite nanoparticles with fibers that offers diverse functionalities for LIB applications. These composite fibers can be fabricated either by a post-treatment of the already synthesized electrospun fibers or by adding the cobalt oxide directly into the electrospun solution. The morphology of these nanofibers can be easily tunable by the control of various electrospinning parameters and also by the heat treatment steps after the fiber formation. The possibility of making 1D NFs with three dimensional (3D) networked structure provides high surface-to-volume ratio to the anode materials and the macro-pores that available in these structure facilitates easy transport of Li^+ ions with reduced diffusion path length, high surface area, easy accommodation of increasing volume changes during cycling and reaction sites. This technique can be combined with other methods such as electrophoretic deposition, hydrothermal and sputtering methods to fabricate dense or porous NFs, core-shell NFs, and hollow structured NFs. Thus, these high-performance battery materials can be combined together so as to get the best advantages of individual materials.

Acknowledgements Authors Dr. Jabeen Fatima M. J and Dr. Raghavan Prasanth, would like to acknowledge the Kerala State Council for Science, Technology, and Environment (KSCSTE), Government of Kerala for financial assistance. Dr. R. Krishnaprya and Dr. R. K. Sharma thank DBT-PAN IIT Centre for Bioenergy (BT/EB/PANIIT/2012) for financial support.

References

1. Chu S, Majumdar A (2012) Opportunities and challenges for a sustainable energy future. Nature 488:294–303. https://doi.org/10.1038/nature11475
2. Goodenough JB, Park KS (2013) The Li-ion rechargeable battery: a perspective. J Am Chem Soc 135:1167–1176. https://doi.org/10.1021/ja3091438
3. Wang W, Tade MO, Shao Z (2015) Research progress of perovskite materials in photocatalysis- and photovoltaics-related energy conversion and environmental treatment. Chem Soc Rev 44:5371–5408. https://doi.org/10.1039/c5cs00113g

4. Balzani V, Credi A, Venturi M (2008) Photochemical conversion of solar energy. Chemsuschem 1:26–58. https://doi.org/10.1002/cssc.200700087
5. Liu C, Li F, Ma LP, Cheng HM (2010) Advanced materials for energy storage. Adv Mater 22:E28–62. https://doi.org/10.1002/adma.200903328
6. Zubi G, Dufo-López R, Carvalho M, Pasaoglu G (2018) The lithium-ion battery: state of the art and future perspectives. Renew Sustain Energy Rev 89:292–308. https://doi.org/10.1016/j.rser.2018.03.002
7. Qi W, Shapter JG, Wu Q, Yin T, Gao G, Cui D (2017) Nanostructured anode materials for lithium-ion batteries: principle, recent progress and future perspectives. J Mater Chem A 5:19521–19540. https://doi.org/10.1039/c7ta05283a
8. Hall PJ, Bain EJ (2008) Energy-storage technologies and electricity generation. Energy Policy 36:4352–4355. https://doi.org/10.1016/j.enpol.2008.09.037
9. Mizushima K, Jones PC, Wiseman PJ, Goodenough JB (1980) Li_xCoO_2 (0 < x~l): a new cathode material for batteries of high energy density. Mat Res Bull 15:783–789
10. Zhang H, Zhao H, Khan MA, Zou W, Xu J, Zhang L, Zhang J (2018) Recent progress in advanced electrode materials, separators and electrolytes for lithium batteries. J Mater Chem A 6:20564–20620. https://doi.org/10.1039/c8ta05336g
11. Winter M, Besenhard JO, Spahr ME, Novak P (1998) Insertion electrode materials for lithium batteries. Adv Mater 10:725–763
12. Ji L, Lin Z, Alcoutlabi M, Zhang X (2011) Recent developments in nanostructured anode materials for rechargeable lithium-ion batteries. Energy Environ Sci 4:5053–5059. https://doi.org/10.1039/c0ee00699h
13. Roy P, Srivastava SK (2015) Nanostructured anode materials for lithium ion batteries. J Mater Chem A 3:2454–2484. https://doi.org/10.1039/c4ta04980b
14. Nitta N, Wu F, Lee JT, Yushin G (2015) Li-ion battery materials: present and future. Mater Today 18:252–264. https://doi.org/10.1016/j.mattod.2014.10.040
15. Tarascon JM, Armand M (2001) Issues and challenges facing rechargeable lithium batteries. Nature 414:359–367. https://doi.org/10.1038/35104644
16. Zhang Y, Liu N (2017) Nanostructured electrode materials for high-energy rechargeable Li, Na and Zn batteries. Chem Mater 29:9589–9604. https://doi.org/10.1021/acs.chemmater.7b03839
17. Canepa P, Sai Gautam G, Hannah DC, Malik R, Liu M, Gallagher KG, Persson KA, Ceder G (2017) Odyssey of multivalent cathode materials: open questions and future challenges. Chem Rev 117:4287–4341. https://doi.org/10.1021/acs.chemrev.6b00614
18. Mai L, Tian X, Xu X, Chang L, Xu L (2014) Nanowire electrodes for electrochemical energy storage devices. Chem Rev 114:11828–11862. https://doi.org/10.1021/cr500177a
19. Dosch H (2001) Some general aspects of confinement in nanomaterials. Appl Surf Sci 182:192–195. https://doi.org/10.1016/S0169-4332(01)00426-3
20. Li D, Xia Y (2004) Electrospinning of nanofibers: reinventing the wheel? Adv Mater 16:1151–1170. https://doi.org/10.1002/adma.200400719
21. Ramakrishna S, Fujihara K, Teo W-E, Yong T, Ma Z, Ramaseshan R (2006) Electrospun nanofibers: solving global issues. Mater Today 9:40–50. https://doi.org/10.1016/s1369-7021(06)71389-x
22. Kenry, Lim CT (2017) Nanofiber technology: current status and emerging developments. Prog Polym Sci 70:1–17. https://doi.org/10.1016/j.progpolymsci.2017.03.002
23. Yarin AL, Koombhongse S, Reneker DH (2001) Taylor cone and jetting from liquid droplets in electrospinning of nanofibers. J Appl Phys 90:4836–4846. https://doi.org/10.1063/1.1408260
24. Lee T-H, Chiu Y-J, Lai Y-C, Fan P-W, Kuo T-Y, Liau I, Chen J-T (2014) Rayleigh-instability-driven morphology transformation of electrospun polymer fibers imaged by in situ optical microscopy and stimulated Raman scattering microscopy. RSC Adv 4:51884–51892. https://doi.org/10.1039/c4ra06228k
25. Dong Z, Kennedy SJ, Wu Y (2011) Electrospinning materials for energy-related applications and devices. J Power Sources 196:4886–4904. https://doi.org/10.1016/j.jpowsour.2011.01.090

26. Fong H, Chun I, Reneker DH (1999) Beaded nanofibers formed during electrospinning. Polymer 40:4585–4592. https://doi.org/10.1016/S0032-3861(99)00068-3
27. Gates DP, Svejda SA, Onate E, Killian CM, Johnson LK, White PS, Brookhart M (2000) Synthesis of branched polyethylene using (R-Diimine)nickel(II) catalysts: influence of temperature, ethylene pressure, and ligand structure on polymer properties. Macromolecules 33:2320–2334
28. Casper CL, Stephens JS, Tassi NG, Chase DB, Rabolt JF (2004) Controlling surface morphology of electrospun polystyrene fibers: Effect of humidity and molecular weight in the electrospinning process. Macromolecules 37:573–578. https://doi.org/10.1021/ma0351975
29. McCann JT, Li D, Xia Y (2005) Electrospinning of nanofibers with core-sheath, hollow, or porous structures. J Mater Chem 15:735–738. https://doi.org/10.1039/b415094e
30. Li D, Wang YL, Xia YN (2003) Electrospinning of polymeric and ceramic nanofibers as uniaxially aligned arrays. Nano Lett 3:1167–1171. https://doi.org/10.1021/nl0344256
31. Fu Z, Li X, Xu G (2014) Novel electrospun SnO_2@carbon nanofibers as high performance anodes for lithium-ion batteries. Cryst Res Technol 49:441–445. https://doi.org/10.1002/crat.201300211
32. Sundaramurthy J, Aravindan V, Suresh Kumar P, Madhavi S, Ramakrishna S (2014) Electrospun TiO_2–δ nanofibers as insertion anode for Li-Ion battery applications. J Phys Chem C 118:16776–16781. https://doi.org/10.1021/jp412787z
33. Wu Q, Zhao R, Zhang X, Li W, Xu R, Diao G, Chen M (2017) Synthesis of flexible Fe_3O_4/C nanofibers with buffering volume expansion performance and their application in lithium-ion batteries. J Power Sources 359:7–16. https://doi.org/10.1016/j.jpowsour.2017.05.020
34. Ou Y, Wen J, Xu H, Xie S, Li J (2013) Ultrafine $LiCoO_2$ powders derived from electrospun nanofibers for Li-ion batteries. J Phys Chem Solids 74:322–327. https://doi.org/10.1016/j.jpcs.2012.10.007
35. Li L, Peng S, Cheah Y, Teh P, Wang J, Wee G, Ko Y, Wong C, Srinivasan M (2013) Electrospun porous $NiCo_2O_4$ nanotubes as advanced electrodes for electrochemical capacitors. Chemistry 19:5892–5898. https://doi.org/10.1002/chem.201204153
36. Li L, Zhu P, Peng S, Srinivasan M, Yan Q, Nair AS, Liu B, Samakrishna S (2014) Controlled growth of cus on electrospun carbon nanofibers as an efficient counter electrode for quantum dot-sensitized solar cells. J Phys Chem C 118:16526–16535. https://doi.org/10.1021/jp4117529
37. Kumuthini R, Ramachandran R, Therese HA, Wang F (2017) Electrochemical properties of electrospun MoS_2@C nanofiber as electrode material for high-performance supercapacitor application. J Alloy Compd 705:624–630. https://doi.org/10.1016/j.jallcom.2017.02.163
38. Ye F, Hou Y, Liu M, Li W, Yang X, Qiu Y, Zhou L, Li H, Xu Y, Zhang Y (2015) Fabrication of mesoporous Li_2S-C nanofibers for high performance Li/Li_2S cell cathodes. Nanoscale 7:9472–9476. https://doi.org/10.1039/c5nr00480b
39. Wu J, Lau W-M, Geng D-S (2017) Recent progress in cobalt-based compounds as high-performance anode materials for lithium ion batteries. Rare Met 36:307–320. https://doi.org/10.1007/s12598-017-0904-y
40. Cao K, Jin T, Yang L, Jiao L (2017) Recent progress in conversion reaction metal oxide anodes for Li-ion batteries. Mater Chem Front 1:2213–2242. https://doi.org/10.1039/c7qm00175d
41. Chen C, Huang Y, Zhang H, Wang X, Wang Y, Jiao L, Yuan H (2016) Controllable synthesis of Cu-doped CoO hierarchical structure for high performance lithium-ion battery. J Power Sources 314:66–75. https://doi.org/10.1016/j.jpowsour.2016.02.085
42. Cao K, Jiao L, Liu Y, Liu H, Wang Y, Yuan H (2015) Ultra-high capacity lithium-ion batteries with hierarchical CoO nanowire clusters as binder free electrodes. Adv Func Mater 25:1082–1089. https://doi.org/10.1002/adfm.201403111
43. Ryu W-H, Shin J, Jung J-W, Kim I-D (2013) Cobalt(ii) monoxide nanoparticles embedded in porous carbon nanofibers as a highly reversible conversion reaction anode for Li-ion batteries. J Mater Chem A 1:3239–3243. https://doi.org/10.1039/c3ta01443f
44. Wang L, Yu Y, Chen P-C, Chen C-H (2008) Electrospun carbon–cobalt composite nanofiber as an anode material for lithium ion batteries. Scripta Mater 58:405–408. https://doi.org/10.1016/j.scriptamat.2007.10.024

45. Zhang M, Uchaker E, Hu S, Zhang Q, Wang T, Cao G, Li J (2013) CoO–carbon nanofiber networks prepared by electrospinning as binder-free anode materials for lithium-ion batteries with enhanced properties. Nanoscale 5:12342–12349. https://doi.org/10.1039/c3nr03931e
46. Zhang M, Yan F, Tang X, Li Q, Wang T, Cao G (2014) Flexible CoO–graphene–carbon nanofiber mats as binder-free anodes for lithium-ion batteries with superior rate capacity and cyclic stability. J Mater Chem A 2:5890–5897. https://doi.org/10.1039/C4TA00311J
47. Wei Y, Yan F, Tang X, Luo Y, Zhang M, Wei W, Chen L (2015) Solvent-controlled synthesis of NiO-CoO/carbon fiber nanobrushes with different densities and their excellent properties for lithium ion storage. ACS Appl Mater Interfaces 7:21703–21711. https://doi.org/10.1021/acsami.5b07233
48. An G-H, Ahn H-J (2014) Carbon nanofiber/cobalt oxide nanopyramid core–shell nanowires for high-performance lithium-ion batteries. J Power Sources 272:828–836. https://doi.org/10.1016/j.jpowsour.2014.09.032
49. Abouali S, Akbari Garakani M, Zhang B, Luo H, Xu Z-L, Huang J-Q, Huang J, Kim J-K (2014) Co3O4/porous electrospun carbon nanofibers as anodes for high performance Li-ion batteries. J Mater Chem A 2:16939–16944. https://doi.org/10.1039/c4ta03206c
50. Park S-H, Lee W-J (2015) Hierarchically mesoporous flower-like cobalt oxide/carbon nanofiber composites with shell–core structure as anodes for lithium ion batteries. Carbon 89:197–207. https://doi.org/10.1016/j.carbon.2015.03.039
51. Hu R, Zhang H, Bu Y, Zhang H, Zhao B, Yang C (2017) Porous Co_3O_4 nanofibers surface-modified by reduced graphene oxide as a durable, high-rate anode for lithium ion battery. Electrochim Acta 228:241–250. https://doi.org/10.1016/j.electacta.2017.01.067
52. Zhang C-L, Lu B-R, Cao F-H, Yu Z-L, Cong H-P, Yu S-H (2018) Hierarchically structured Co3O4@carbon porous fibers derived from electrospun ZIF-67/PAN nanofibers as anodes for lithium ion batteries. J Mater Chem A 6:12962–12968. https://doi.org/10.1039/c8ta03397h
53. Chen M, Xia X, Yin J, Chen Q (2015) Construction of Co_3O_4 nanotubes as high-performance anode material for lithium ion batteries. Electrochim Acta 160:15–21. https://doi.org/10.1016/j.electacta.2015.02.055
54. Liu J, Fu B, Dai J, Zhu X, Wang Q (2019) Study the mechanism of enhanced Li storage capacity through decreasing internal resistance by high electronical conductivity via sol-gel electrospinning of Co_3O_4 carbon nanofibers. ChemistrySelect 4:3542–3546. https://doi.org/10.1002/slct.201804041
55. Wang R, Wu J (2017) Structure and basic properties of ternary metal oxides and their prospects for application in supercapacitors. In: Metal oxides in supercapacitors, pp 99–132
56. Yuan C, Wu HB, Xie Y, Lou XW (2014) Mixed transition-metal oxides: design, synthesis, and energy-related applications. Angew Chem Int Ed Engl 53:1488–1504. https://doi.org/10.1002/anie.201303971
57. Marco JF, Gancedo JR, Gracia M, Gautier JL, Ríos E, Berry FJ (2000) Characterization of the nickel cobaltite, $NiCo_2O_4$, prepared by several methods: an XRD, XANES, EXAFS, and XPS study. J Solid State Chem 153:74–81. https://doi.org/10.1006/jssc.2000.8749
58. Zhou G, Wu C, Wei Y, Li C, Lian Q, Cui C, Wei W, Chen L (2016) Tufted $NiCo_2O_4$ nanoneedles grown on carbon nanofibers with advanced electrochemical property for lithium ion batteries. Electrochim Acta 222:1878–1886. https://doi.org/10.1016/j.electacta.2016.12.001
59. Zhu J, Xu Z, Lu B (2014) Ultrafine Au nanoparticles decorated $NiCo_2O_4$ nanotubes as anode material for high-performance supercapacitor and lithium-ion battery applications. Nano Energy 7:114–123. https://doi.org/10.1016/j.nanoen.2014.04.010
60. Syu J-M, Hsiao M-L, Lo C-T (2017) Electrospun carbon fiber/Ni–Co composites as binder-free anodes for lithium-ion batteries. J Electrochem Soc 164:A3903–A3913. https://doi.org/10.1149/2.0021802jes
61. Luo W, Hu X, Sun Y, Huang Y (2012) Electrospun porous $ZnCo_2O_4$ nanotubes as a high-performance anode material for lithium-ion batteries. J Mater Chem 22:8916–8921. https://doi.org/10.1039/c2jm00094f
62. Chen R, Hu Y, Shen Z, Chen Y, He X, Zhang X, Zhang Y (2016) Controlled synthesis of carbon nanofibers anchored with $Zn(x)Co(3-x)O_4$ nanocubes as binder-free anode materials

for lithium-ion batteries. ACS Appl Mater Interfaces 8:2591–2599. https://doi.org/10.1021/acsami.5b10340
63. Yang G, Xu X, Yan W, Yang H, Ding S (2014) Single-spinneret electrospinning fabrication of $CoMn_2O_4$ hollow nanofibers with excellent performance in lithium-ion batteries. Electrochim Acta 137:462–469. https://doi.org/10.1016/j.electacta.2014.05.167
64. Hwang SM, Kim SY, Kim JG, Kim KJ, Lee JW, Park MS, Kim YJ, Shahabuddin M, Yamauchi Y, Kim JH (2015) Electrospun manganese-cobalt oxide hollow nanofibres synthesized via combustion reactions and their lithium storage performance. Nanoscale 7:8351–8355. https://doi.org/10.1039/c5nr01145k
65. Zhang G, Lou XW (2013) General solution growth of mesoporous $NiCo_2O_4$ nanosheets on various conductive substrates as high-performance electrodes for supercapacitors. Adv Mater 25:976–979. https://doi.org/10.1002/adma.201204128